Comprehensive estimation of nuclide production cross sections using a phenomenological approach

Hiroki Iwamoto ●*

Nuclear Science and Engineering Center, Japan Atomic Energy Agency (JAEA),
2-4 Shirakata, Tokai-mura, Naka-gun, Ibaraki 319-1195, Japan

Shin-ichiro Meigo ●

J-PARC Center, Japan Atomic Energy Agency (JAEA),
2-4 Shirakata, Tokai-mura, Naka-gun, Ibaraki 319-1195, Japan

Kenta Sugihara ●

Radiation Science Center, High Energy Accelerator Research Organization (KEK), 1-1 Oho, Tsukuba, Ibaraki 305-0801, Japan
and The Graduate University for Advanced Studies (SOKENDAI), Hayama, Kanagawa 240-0193, Japan

Nuclide production cross sections are crucial in nuclear research, development, space exploration, and astrophysical investigations. Despite their importance, limited experimental data availability restricts the practicality of phenomenological approaches to comprehensive cross-section estimation. To address this, we propose a Gaussian process-based machine learning (ML) model capable of transferring knowledge from elements with abundant data to those with limited or no experimental data. Our ML model not only enables comprehensive cross-section estimations for various elements but also demonstrates predictive capabilities akin to physics models, even in regions with scarce training data.

I. INTRODUCTION

Cross-section data for nuclear reactions, specifically nuclide production cross sections, are fundamental for nuclear research, development, space exploration, and astrophysical investigations [1–11]. These research areas demand comprehensive and reliable data at varying precision levels. Theoretical and semiempirical models (e.g., [12–23]) play an indispensable role in understanding nuclear reaction mechanisms and predicting cross sections. However, with ample experimental data, accurate cross-section estimation can be achieved through a phenomenological approach eliminating the need for these theoretical and semiempirical models (e.g., [24–26]). Unfortunately, such data are available only for restricted reaction channels and a restricted range of incident energies in a very small number of materials, limiting the practicality of a phenomenological approach to comprehensive cross-section estimation.

To address these limitations, this paper introduces a machine learning (ML) model, utilizing the Gaussian process (GP) [27]. This model, an extension of our GP regression model [28,29] to a transfer learning framework, transcends the challenges of the phenomenological approach by transferring knowledge from target elements with abundant experimental data to those with limited or no experimental data.

The developed model not only facilitates comprehensive cross-section estimations, including uncertainties, for target elements but also demonstrates predictive capabilities comparable to physics models, even in regions where experimental data used for training are scarce. To the best of our knowledge, this is the first effort to comprehensively estimate nuclide production cross sections in a fully phenomenological manner.

In Sec. II, we introduce our ML model, leveraging transfer learning. In Sec. III, we explore the limitations of conventional GP regression models and compare them with physics model analyses to specifically highlight the effectiveness of our approach and address associated challenges. Here, we focus on the cross sections of beryllium-7 (^{7}Be) and tritium (^{3}H) production resulting from proton-induced nuclear reactions, targeting elements from C to Bi. For the physics model, we employ the Monte Carlo spallation model INCL4.6/GEM, incorporated into the Particle and Heavy Ion Transport code System (PHITS) version 3.30 [30]. This model, suitable for nuclear reaction simulation spanning the MeV to GeV energy range, combines the generalized evaporation model (GEM) [31] and the Liège intranuclear cascade model version 4.6 (INCL4.6) [32], describing the production of nuclides and secondary particles. Its accuracy has been validated through benchmark analyses [33–36]. Note that since our focus is on demonstrating the applicability of the developed ML model, we exclusively compare it with INCL4.6/GEM. Furthermore, we showcase the estimation capability of our ML model using experimental data. Finally, Sec. IV provides a summary of
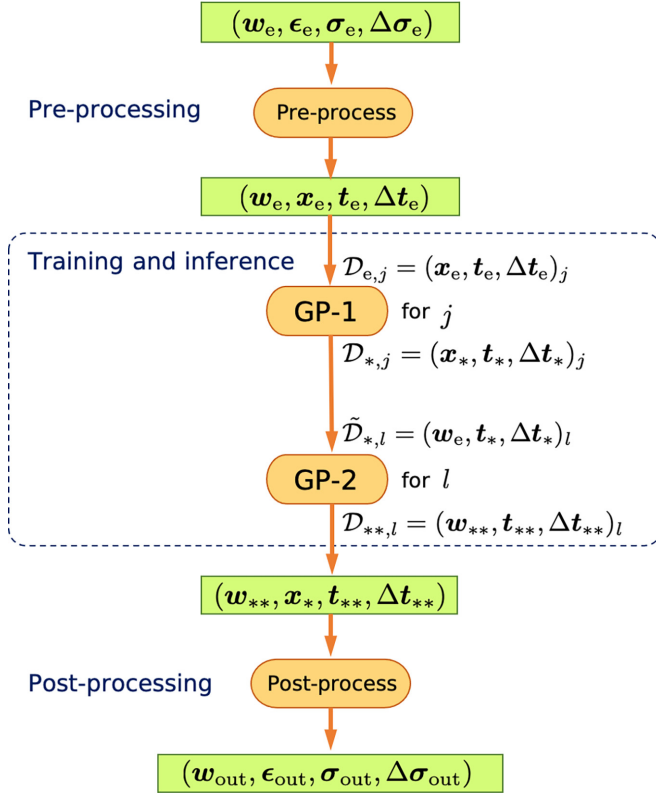
*iwamoto.hiroki@jaea.go.jp

FIG. 1. Cross-section data flow in the developed model.

FIG. 2. Proton-induced ^{7}Be production cross sections for Al (left) and Mo (right) generated by GP-1. The blue dot-dashed lines (GP-1) represent the generated nominal value with its 1σ uncertainty. The green dot-dashed lines indicate analytical values with INCL4.6/GEM. The gray points with error bars indicate the experimental cross-section data with 1σ measurement uncertainty.

the study, highlighting key findings, and offer suggestions for future research.

II. MODEL

A. Experimental data employed

We obtained experimental data from the experimental nuclear reaction database EXFOR [37] and those recently measured by the authors at J-PARC [38,39], corresponding to each target element and produced nuclide. Most nuclide production cross-section measurements have been conducted on targets with natural abundance, and there is limited experimental data on enriched targets. Therefore, this study utilized only experimental data for targets with natural abundance.

While the typical process of nuclear data evaluation in the evaluated nuclear data libraries (e.g., ENDF [40] and JENDL [41]) involves a thorough examination of the experimental data to determine its acceptability, we chose to use the data registered in EXFOR as directly as possible in order to focus on the applicability of our ML model to cross-section estimation. Even if measurement uncertainties are revisited in the future or the experimental data employed undergo slight changes, they will not significantly alter the applicability of our model. As demonstrated in our prior work [28], the measurement uncertainty of experimental values affects the cross-section estimations by our GP regression model. Therefore, only experimental data
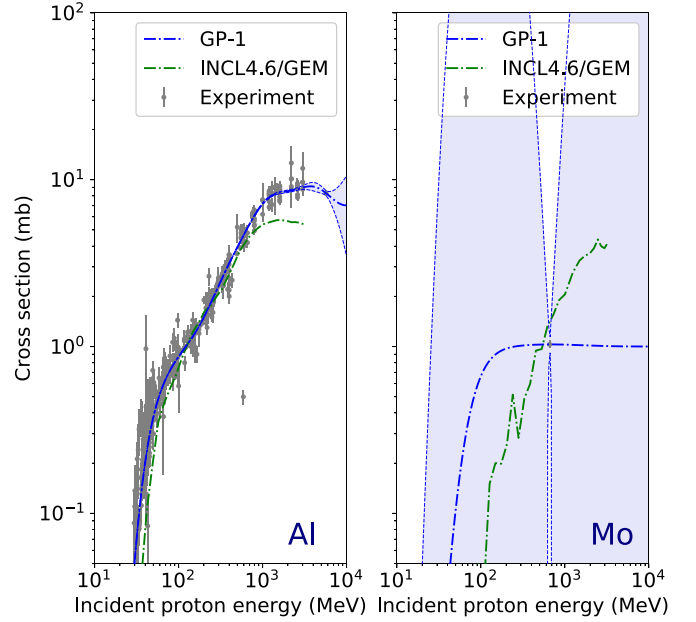
for which measurement uncertainty was evaluated were employed.

The obtained data set for target element j is denoted as $\{\epsilon_e, \sigma_e, \Delta\sigma_e \mid \epsilon_{e,i}, \sigma_{e,i}, \Delta\sigma_{e,i}, i = 1, ..., I\}_j$, where I denotes the number of the experimental data points for j. Here, ϵ_e, σ_e, and $\Delta\sigma_e$ indicate the incident proton energy in MeV, cross section in mb, and its uncertainty in mb, respectively.

B. Pre-processing

Figure 1 depicts a cross-section data flow in our ML model, comprising three stages: pre-processing, training and inference, and postprocessing. In the preprocessing stage, the cross section and its uncertainty undergo a logarithmic transformation to avoid negative estimates, as $t_e = \log_{10}\sigma_e$ and $\Delta t_e = \log_{10}(\sigma_e + \Delta\sigma_e) - t_e$, where $\{t_e, \Delta t_e \mid t_{e,i}, \Delta t_{e,i}, i = 1, \dots, I\}_j$. Given the target energy spans from MeV to GeV range, the energy is logarithmically transformed using the natural logarithm, as $x_e = \ln\epsilon_e$, where $\{x_e \mid x_{e,i}, i = 1, \dots, I\}_j$. Our ML model utilizes these transformed data sets $\mathcal{D}_{e,j} = (x_e, t_e, \Delta t_e)_j$ alongside the atomic mass of the target element $\{w_e \mid w_{e,j}, j = 1, ..., J\}$ as the input data sets of the subsequent stage, where J indicates the number of elements that have experimental data.

C. Training and inference

The training and inference stage comprises two processes. These processes are accomplished by two GP modules: GP-1, which initially estimates nuclide production cross sections for target elements with available experimental values, and GP-2,

TABLE I. EXFOR entry numbers and references for proton-induced ^{7}Be-production cross-section data for targets from C to Bi.

Target	I	EXFOR entry number
C	97	C0235 [43], C0255 [44], C0261 [45], D0640 [46], O0073 [47], O0277 [48], O0284 [49], O0729 [50], O2474 [51], X0000 [38]
N	72	A0485 [52], D0640 [46], O0277 [48], O0282 [53], O0284 [49], O0414 [54], O0729 [50], O0871 [55], O2000 [56]
O	34	D0640 [46], O0073 [47], O0277 [48], O0282 [53], O0729 [50], O2250 [57]
F	45	A0485 [52], C0061 [58], C0220 [59], O0276 [60], O0729 [50], O2134 [61]
Na	25	A0485 [52], C0220 [59], O0554 [62], O0729 [50]
Mg	154	A0485 [52], C0196 [63], C1508 [64], O0073 [47], O0077 [65], O0078 [66], O0094 [67], O0276 [60], O0277 [48], O0282 [53], O0284 [49], O0501 [68], O2056 [69], O2134 [61]
Al	536	A0340 [70], A0902 [71], A0917 [72], B0085 [73], C0196 [63], C0220 [59], C0255 [44], C0261 [45], C0265 [74], C0461 [75], C2368 [76], D0028 [77], D0054 [78], D0505 [79], D0640 [46], D4384 [80], C0401 [81], E0057 [82], E1829 [83], E2665 [84], E2667 [85], F1215 [86], O0078 [66], O0276 [60], O0277 [48], O0282 [53], O0284 [49], O0501 [68], O0554 [62], O0729 [50], O0985 [87], O1728 [88], O2056 [69], O2128 [89], O2134 [61], X0000 [38]
Si	135	C0507 [90], D0640 [46], O0078 [66], O0094 [67], O0276 [60], O0277 [48], O0282 [53], O0284 [49], O0554 [62], O0729 [50], O2037 [91], O2056 [69], O2134 [61]
P	6	O0554 [62], O0729 [50]
S	6	O0554 [62], O0729 [50]
Cl	5	O0729 [50]
Ar	4	A0928 [92], C1962 [93]
Ca	5	O0729 [50]
Sc	4	X0000 [38]
Ti	25	A0501 [94], A0512 [95], C0271 [96], C0401 [81], O0078 [66], O0276 [60], O0277 [48], O0284 [49], O1882 [97], X0001 [39]
V	16	C2366 [98], D0054 [78], O0277 [48], O2128 [89], X0000 [38]
Cr	11	A0901 [99]
Mn	12	D0640 [46], E2719 [100], O0078 [66], O0277 [48], O0284 [49]
Fe	86	A0501 [94], C0401 [81], O0073 [47], O0078 [66], O0085 [101], O0094 [67], O0276 [60], O0277 [48], O0283 [102], O0284 [49], O0299 [103], O0729 [50], O1881 [104], O1882 [97], O2037 [91], T0131 [105]
Co	20	A0501 [94], C0401 [81], C2110 [106], D0640 [46], E2719 [100], O0078 [66], O0277 [48], O0284 [49], O0397 [107]
Ni	46	A0906 [108], E2731 [109], C0401 [81], O0073 [47], O0077 [65], O0078 [66], O0094 [67], O0114 [110], O0276 [60], O0277 [48], O0284 [49], O1882 [97]
Cu	33	A0501 [94], C0255 [44], C0401 [81], O0078 [66], O0276 [60], O0277 [48], O0284 [49], O0542 [111], O0722 [112], T0131 [105]
Zn	7	E1243 [113], E1251 [114], O0722 [112]
Ge	1	A0512 [95]
Y	14	D0640 [46], O0078 [66], O0204 [115], O0276 [60]
Zr	21	A0513 [116], D0640 [46], E2731 [109], O0204 [115], O0276 [60]
Nb	25	A0491 [117], D0054 [78], D0640 [46], O0276 [60], O0981 [118], X0001 [39]
Mo	1	A0557 [119]
Tc	4	O0985 [87]
Rh	1	D0640 [46]
Ag	6	C0401 [81], C2109 [120], C2340 [121], C2351 [122], F1312 [123]
In	1	C0342 [124]
Sb	1	A0917 [72]
Hf	1	A0822 [125]
Ta	7	A0904 [126]
W	12	A0721 [127], O0781 [128], O0800 [129], O1099 [130]
Re	4	O2139 [131]
Au	15	A0491 [117], D0054 [78], O0276 [60], O2128 [89]
Pb	19	A0927 [132], O0500 [133], O1728 [88]
Bi	7	O1728 [88]

which estimates nuclide production cross sections for energy points based on the target atomic mass using the previously estimated cross sections. When experimental data is input into this stage, the two learning models assimilate the information and generate cross-section outputs for any target element and incident proton energy.

In the first process, a data set for target element j, $\mathcal{D}_{*,j} = (\boldsymbol{x}_*, \boldsymbol{t}_*, \Delta\boldsymbol{t}_*)_j$, where $\{x_*, t_*, \Delta t_* \mid x_{*,l}, t_{*,l}, \Delta t_{*,l}, l = 1, \ldots, L\}$, is generated as a function of $\boldsymbol{x}$, with $\mathcal{D}_{e,j}$ serving as the training data, where L is the number of energy points. To prevent the cross section from diverging below the threshold energy, an inducing point with a small cross-section value at 10 MeV, considered below the threshold energy for the targets of interest, was included in the training data set, as in our previous work [29]. The GP-1 defines that the observed value $\boldsymbol{y}_*$ at $\boldsymbol{x}_*$, given $\mathcal{D}_{e,j}$, follows a normal distribution with mean $\mu(\boldsymbol{x}_*)$ $(\equiv \boldsymbol{\mu}_*)$ and covariance $\Sigma(\boldsymbol{x}_*, \boldsymbol{x}_*)$ $(\equiv \boldsymbol{\Sigma}_*)$:

$$p(\boldsymbol{y}_*|\mathcal{D}_{e,j}) = \mathcal{N}(\boldsymbol{\mu}_*, \boldsymbol{\Sigma}_*), \tag{1}$$

where

$$\boldsymbol{\mu}_* = \boldsymbol{k}_{LI}^\top \boldsymbol{k}_{II}^{-1} \boldsymbol{t}_I, \tag{2}$$

$$\boldsymbol{\Sigma}_* = \boldsymbol{k}_{LL} - \boldsymbol{k}_{LI}^\top (\boldsymbol{k}_{II} + \boldsymbol{n}_{II})^{-1} \boldsymbol{k}_{IL}. \tag{3}$$

In these equations, we define $\boldsymbol{t}_I$ as $\boldsymbol{t}_e$; $\boldsymbol{k}_{LI}$ (equivalent to $\boldsymbol{k}_{IL}$) as $\kappa(\boldsymbol{x}_*, \boldsymbol{x}_e)$, $\boldsymbol{k}_{II}$ as $\kappa(\boldsymbol{x}_e, \boldsymbol{x}_e)$, and $\boldsymbol{k}_{LL}$ as $\kappa(\boldsymbol{x}_*, \boldsymbol{x}_*)$, where κ represents kernel functions. The behavior of the mean and covariance among the training data depends on the chosen kernel function. In GP-1, we utilized the radial basis function (RBF) kernel to ensure a smooth function. The noise term $\boldsymbol{n}_{II}$ is defined as $\boldsymbol{n}_{II} = \mathrm{diag}((\Delta\boldsymbol{t}_e)^2)$. Here, we define the nominal value $\boldsymbol{t}_*$ as $\boldsymbol{\mu}_*$ and its 1σ uncertainty $\Delta\boldsymbol{t}_*$ as $\sqrt{\mathrm{diag}(\boldsymbol{\Sigma}_*)}$. These operations apply to J target elements.

In the second process, the same operation as in GP-1 is performed for $\boldsymbol{w}$ instead of $\boldsymbol{x}$. A data set for incident energy l, $\mathcal{D}_{**,l} = (\boldsymbol{w}_{**}, \boldsymbol{t}_{**}, \Delta\boldsymbol{t}_{**})_l$ where $\{w_{**}, t_{**}, \Delta t_{**} \mid w_{**,m}, t_{**,m}, \Delta t_{**,m}, m = 1, \ldots, M\}$, is generated as a function of $\boldsymbol{w}$, with $\tilde{\mathcal{D}}_{*,l} = (\boldsymbol{w}_e, \boldsymbol{t}_*, \Delta\boldsymbol{t}_*)_l$ serving as the training data, where M is the number of atomic mass points. The GP-2 defines that the observed value $\boldsymbol{y}_{**}$ at $\boldsymbol{w}_{**}$ given $\mathcal{D}_{*,l}$, follows a normal distribution with mean $\mu(\boldsymbol{w}_{**})$ $(\equiv \boldsymbol{\mu}_{**})$ and covariance $\Sigma(\boldsymbol{w}_{**}, \boldsymbol{w}_{**})$ $(\equiv \boldsymbol{\Sigma}_{**})$:

$$p(\boldsymbol{y}_{**}|\tilde{\mathcal{D}}_{*,l}) = \mathcal{N}(\boldsymbol{\mu}_{**}, \boldsymbol{\Sigma}_{**}), \tag{4}$$

where

$$\boldsymbol{\mu}_{**} = \boldsymbol{k}_{ML}^\top \boldsymbol{k}_{LL}^{-1} \boldsymbol{t}_L, \tag{5}$$

$$\boldsymbol{\Sigma}_{**} = \boldsymbol{k}_{MM} - \boldsymbol{k}_{ML}^\top (\boldsymbol{k}_{LL} + \boldsymbol{n}_{LL})^{-1} \boldsymbol{k}_{LM}. \tag{6}$$

In these equations, we define $\boldsymbol{t}_L$ as $\boldsymbol{t}_*$; $\boldsymbol{k}_{ML}$ (equivalent to $\boldsymbol{k}_{LM}$) as $\kappa(\boldsymbol{w}_{**}, \boldsymbol{w}_*)$, $\boldsymbol{k}_{LL}$ as $\kappa(\boldsymbol{w}_*, \boldsymbol{w}_*)$, and $\boldsymbol{k}_{MM}$ as $\kappa(\boldsymbol{w}_{**}, \boldsymbol{w}_{**})$. In GP-2, we employed the Matérn 3/2 (M$_{3/2}$) kernel for κ to reasonably interpolate the atomic mass range from 120 u to 170 u, where no training data exists. The noise term $\boldsymbol{n}_{LL}$ is defined as $\boldsymbol{n}_{LL} = c_0 \cdot \mathrm{diag}((\Delta\boldsymbol{t}_*)^2)$. Here, we have adopted $c_0 = 5$ to ensure a plausible fitting. Additionally, we introduce the nominal value $\boldsymbol{t}_{**}$ as $\boldsymbol{\mu}_{**}$ and its 1σ uncertainty $\Delta\boldsymbol{t}_{**}$ as $\sqrt{\mathrm{diag}(\boldsymbol{\Sigma}_{**})}$. These operations are performed for L energy points.
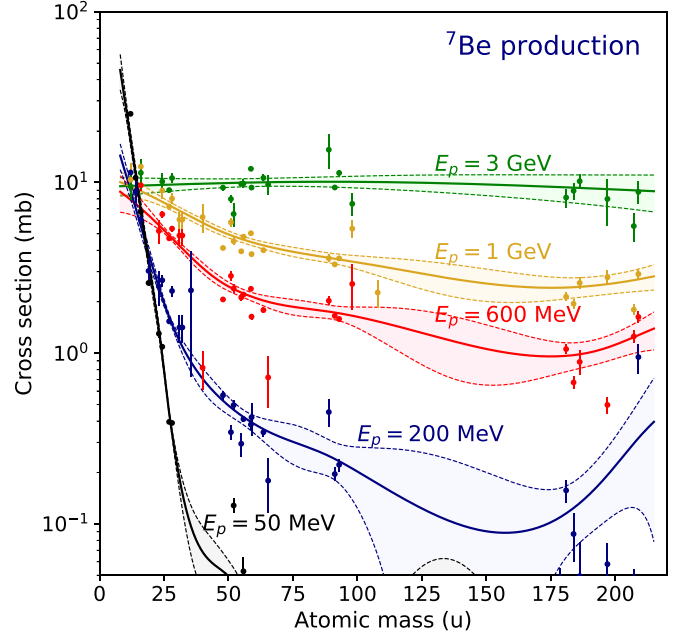

FIG. 3. Proton-induced ^{7}Be production cross sections for the incident proton energies of 50 MeV, 200 MeV, 600 MeV, 1 GeV, and 3 GeV against the target atomic mass, generated by GP-1 and GP-2. The line with a band for each incident proton energy represents the generated nominal value with its 1σ uncertainty. The points with error bars show the cross-section data with uncertainty generated by GP-1.

In ML, methods such as cross-validation and grid search are often used to obtain hyperparameters with high generalization performance. On the other hand, GPs achieve excellent generalization by maximizing the marginal likelihood within their Bayesian framework. Therefore, both GP-1 and GP-2 employ this latter method. To solve the maximization problem, we utilized a constrained gradient method called L-BFGS-B [42], aimed at preventing excessively small length scales of the employed kernel functions.

D. Postprocessing

In the postprocessing stage, the data set generated through GP-1 and GP-2 is scaled back to its original scale: $\boldsymbol{\epsilon}_* = e^{\boldsymbol{x}_*}$, $\boldsymbol{\sigma}_* = 10^{\boldsymbol{t}_*}$, and $\Delta\boldsymbol{\sigma}_* = 10^{(\boldsymbol{t}_* + \Delta\boldsymbol{t}_*)} - \boldsymbol{\sigma}_*$, and then an output data set $\mathcal{D}_{\mathrm{out}} = (\boldsymbol{w}_{\mathrm{out}}, \boldsymbol{\epsilon}_{\mathrm{out}}, \boldsymbol{\sigma}_{\mathrm{out}}, \Delta\boldsymbol{\sigma}_{\mathrm{out}})$ is obtained, where $\{w_{\mathrm{out}} \mid w_{**,m}, m = 1, \ldots, M\}$ and $\{\epsilon_{\mathrm{out}}, \sigma_{\mathrm{out}}, \Delta\sigma_{\mathrm{out}} \mid \epsilon_{*,l}, \sigma_{**,l}, \Delta\sigma_{**,l}, l = 1, \ldots, L\}$.

III. RESULTS AND DISCUSSION

A. ^{7}Be production cross sections

Tables I provide a summary of EXFOR entry numbers and references for experimental data extracted from the EX-FOR database regarding the proton-induced ^{7}Be production cross-section data. 'I' in the table denotes the total number of experimental data points for each target. X0000 [38] and X0001 [39] are not currently registered in EXFOR and represent our most recently acquired data. A combined total of 1524 points from these entries and our own data were utilized
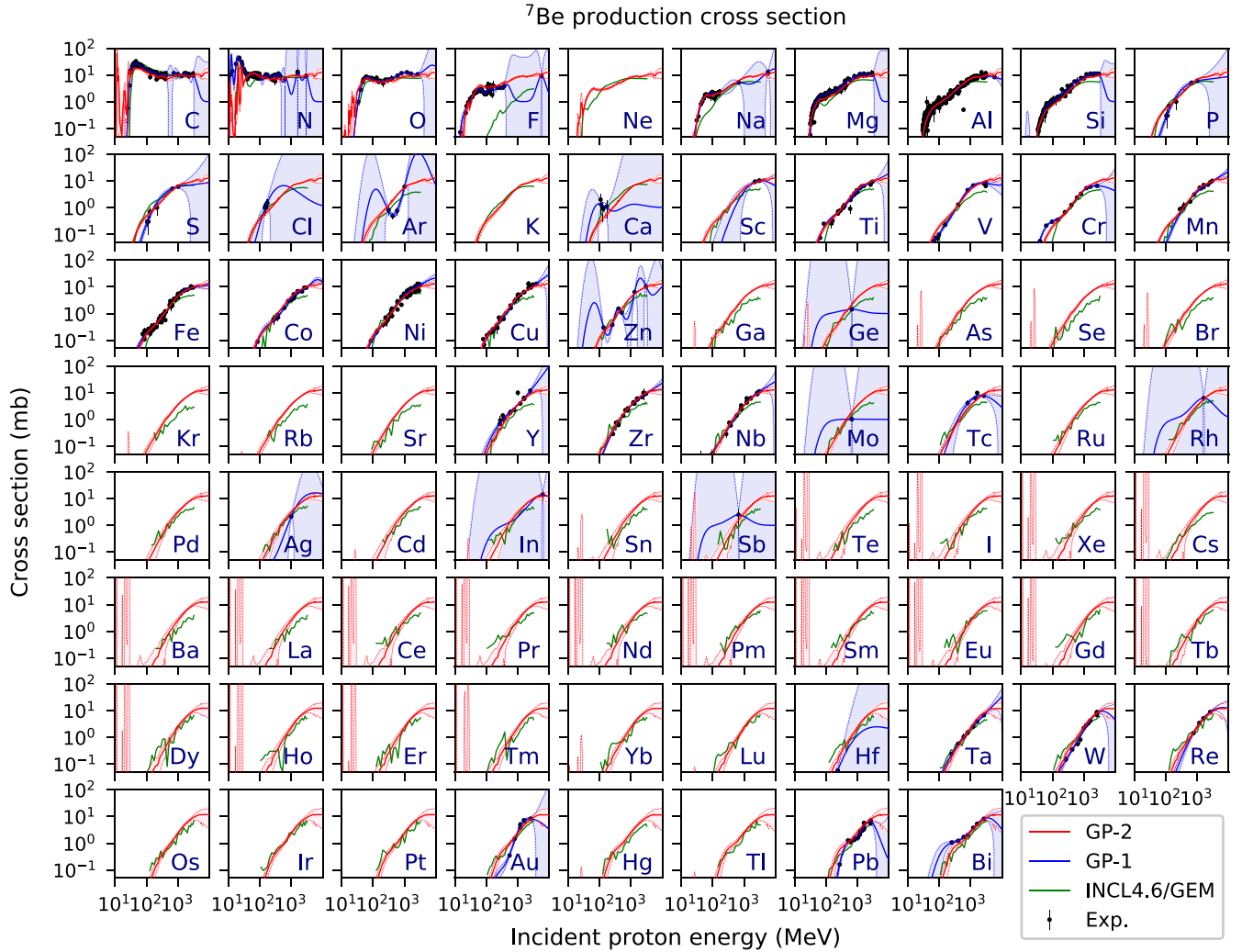
FIG. 4. Proton-induced ^{7}Be production cross sections over target elements from C to Bi. The blue lines (GP-1) represent nominal values with 1σ uncertainty obtained by GP-1 learning. The red lines (GP-2) represent values generated from GP-2 learning. The green lines show analytical values using INCL4.6/GEM. The points with error bars represent experimental cross-section data with 1σ measurement uncertainty.

to train the model. The table illustrates a significant imbalance in the availability of experimental data for each target.

Figure 2 compares GP-1 regression results for the proton-induced ^{7}Be production cross sections, using Al and Mo as examples with and without ample experimental data, where a data point of $(\epsilon_e, \sigma_e, \Delta\sigma_e) = (10, 1 \times 10^{-5}, 2 \times 10^{-6})$ was given as the inducing point. The figure also includes results from INCL4.6/GEM at incident proton energies up to 3 GeV. Abundant experimental data for the Al target allow GP-1 to reasonably estimate cross sections from the threshold energy to 10 GeV. Because our ML model derives cross sections phenomenologically from experimental values, it exhibits better agreement with experimental data than with analytical values from the physics model, as indicated by our previous study [28]. However, due to only one available data set for the Mo target [119], the GP produces highly uncertain results. Figure 3 displays the atomic mass distribution of cross-section estimates at specific incident energies. These estimates were derived by GP-2 learning from GP-1 results for a total of 40 target elements with available experimental data, ranging

from C to Bi (see Table I). Points accompanied by error bars correspond to cross sections produced by GP-1. To enhance clarity, data with an uncertainty margin exceeding 80% have been excluded for ease of interpretation. The ^{7}Be production cross section data for B and Li, exhibiting significant individuality in their excitation functions, were omitted from the GP-2 process due to their adverse impact on the transferability of cross-section estimates between targets in GP-2. It is observed that, within the atomic mass range of 120 u to 170 u, GP-2 successfully interpolates the cross-section data, even in the absence of experimental data. The figure reveals the following trends: Except for a few light target elements, ^{7}Be is more likely to be produced at high incident energies. Heavier target elements result in less ^{7}Be production. Above 1 GeV, production saturates at an almost constant value (~ 10 mb), regardless of the target mass. As demonstrated later, the physics model exhibit similar trends.

Figure 4 presents proton-induced ^{7}Be production cross sections for target elements ranging from C to Bi, obtained through GP-1 and GP-2, plotted against incident proton
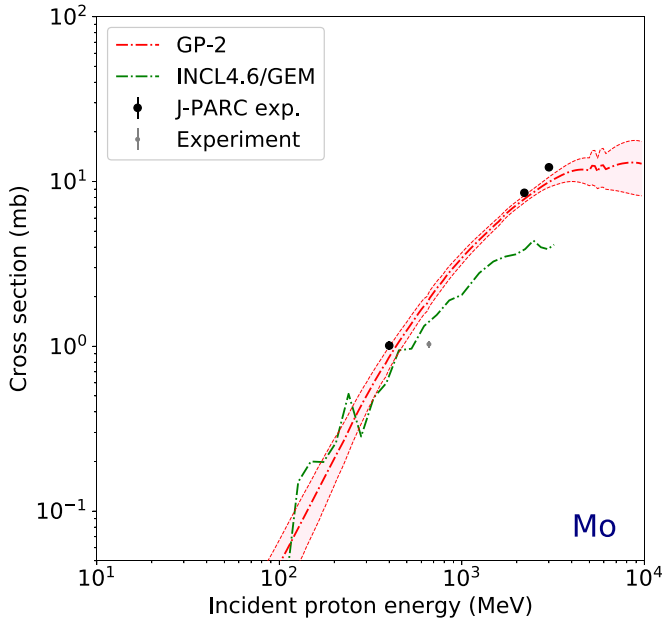
FIG. 5. Proton-induced ^{7}Be production cross sections of Mo generated from GP-2 (red dot-dashed line with band) compared with recent preliminary data measured at J-PARC (black points with error bars), which are not used for training. The green dot-dashed line indicates analytical values using INCL4.6/GEM.

FIG. 6. Proton-induced ^{7}Be production cross sections of Fe generated from GP-2 excluding the Fe experimental data for training data (red dot-dashed line with band). The green dot-dashed line indicates analytical values with INCL4.6/GEM. The gray points with error bars indicate the experimental cross-section data with 1σ measurement uncertainty.

energy from 10 MeV to 10 GeV. The blue lines accompanied by 1σ uncertainty bands represent results exclusively from GP-1 and is relevant to target elements with available experimental data. In contrast, the red lines, also with 1σ uncertainty bands, represent results from GP-2, extending its applicability
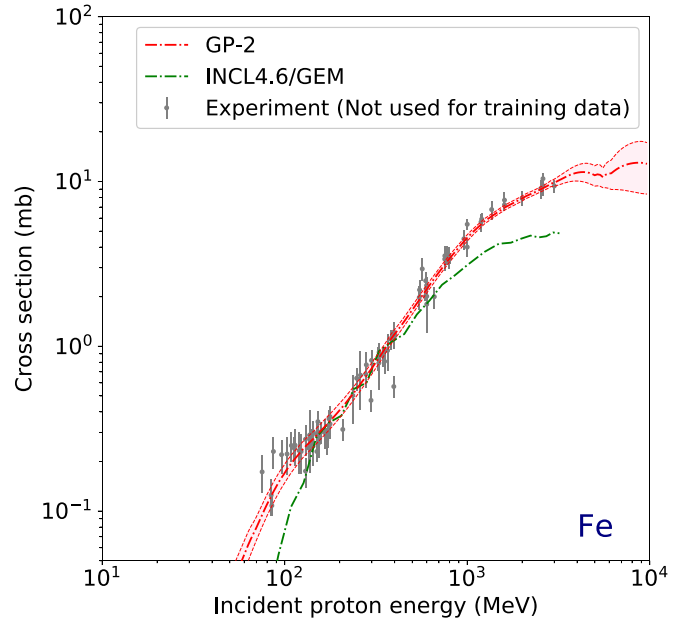
to all target elements. As shown in this figure, GP-2 produces plausible cross-section shapes for all target elements from C to Bi. It also provides reasonable shapes for elements where experimental data are unavailable and cannot be estimated by

TABLE II. EXFOR entry numbers and references for the proton-induced ^{3}H production cross-section data.

Target	I	EXFOR entry number
C	10	O0235 [43], O0304 [134], O0305 [135], O0342 [136]
N	4	C0235 [43], C0836 [137], O0305 [135]
O	4	C0235 [43], O0305 [135]
Mg	6	A0877 [138], C0836 [137], D0628 [139]
Al	30	C0116 [140], D0628 [139], F1477 [141], O0304 [134], O0313 [142], C0836 [137], E1854 [143], O0044 [144], O0305 [135]
Si	3	D0628 [139], O0529 [145]
V	1	D0628 [139]
Cr	1	D0628 [139]
Mn	1	D0628 [139]
Fe	16	C0277 [146], C0836 [137], D0627 [147], D0628 [139], O0304 [134], O0305 [135], O0342 [136]
Ni	15	C0836 [137], D0628 [139], F1477 [141]
Zn	1	A0877 [138]
Nb	2	E1854 [143], O0342 [136]
Cd	1	A0877 [138]
Sn	7	E1854 [143], O0305 [135], O0313 [142], O0342 [136]
Sb	1	A0877 [138]
Ag	4	A0877 [138], C0836 [137], D0628 [139], E1854 [143]
W	11	F1477 [141]
Au	14	A0877 [138], D0512 [148], E1854 [143], O0044 [144], O0342 [136]
Pb	11	C0836 [137], D0628 [139], E1854 [143], O0305 [135], O0313 [142]
Bi	7	A0877 [138], D0628 [139], O0313 [142]
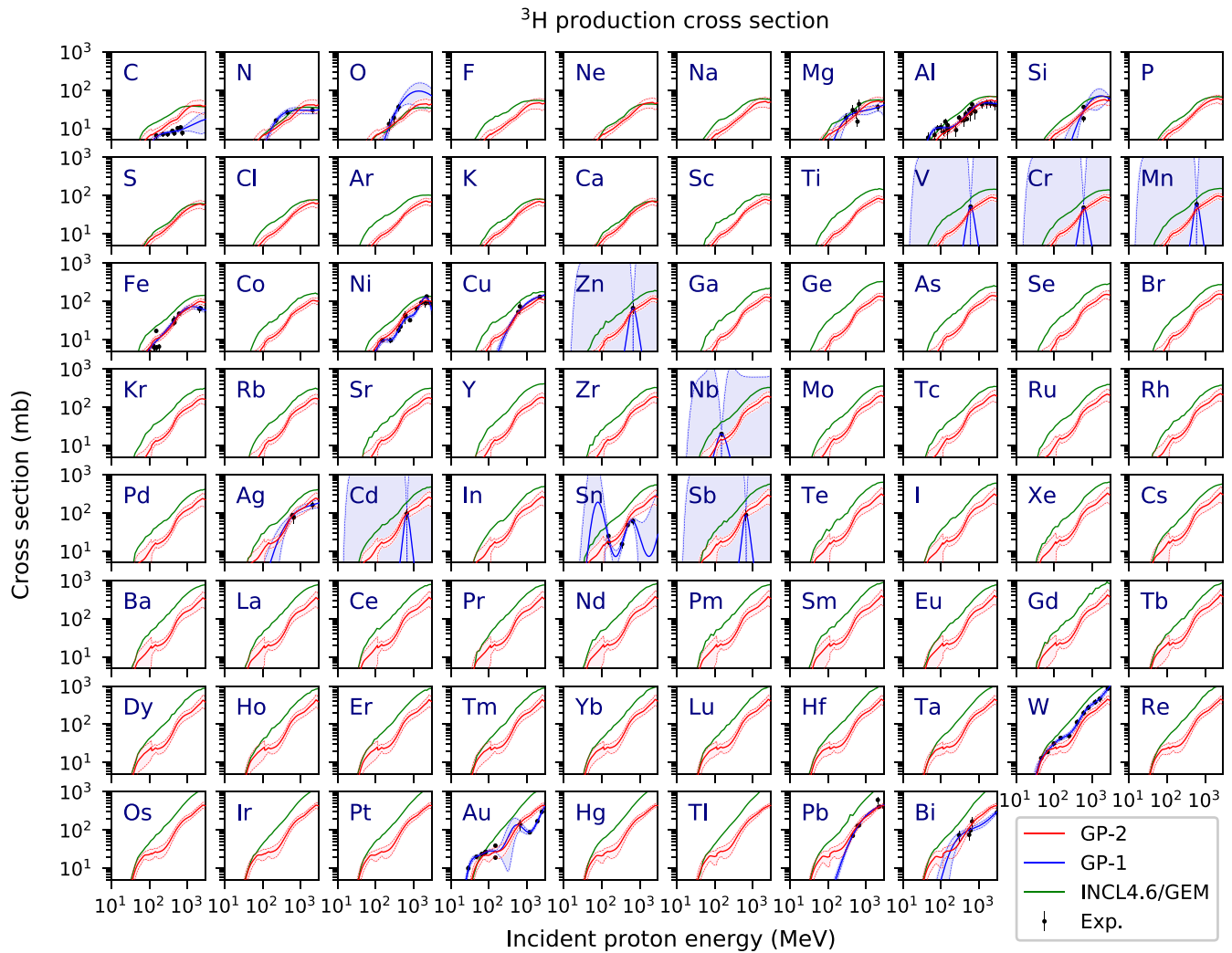
FIG. 7. Same as Fig. 4 but for ^{3}H production.

GP-1 such as elements from Te to Lu, those with only one data point resulting in a large uncertainty estimate such as Ge, Mo, and Re. This is because of the assumption of similarity in cross-section shapes among adjacent targets based on the target mass number. The reduced reproducibility of GP-2 for cross sections below 50 MeV for C, N, and O compared to GP-1 results is attributed to the lack of similarity between these target elements. In such cases, it is advisable to adopt results from GP-1.

It is important to highlight that although the cross-section shapes resemble those obtained from the physics model analysis, our ML model distinctly outperforms in reproducing the experimental values. Additionally, unlike Monte Carlo–based physics models like INCL4.6/GEM, which demand extensive computational resources for analyses at each incident energy point and target element to achieve adequate statistics, our ML model completes the task in a few seconds to a few minutes of parallel computation, contingent on the number of experimental data points.

In Fig. 5, we compare the estimated ^{7}Be production cross section of the Mo target based on the experimental data

from Table I with recent preliminary data obtained at J-PARC, which will be reported along with data for other nuclides in the future. The physics model underestimates the experimental data in high-energy region, but our ML model successfully reproduces the experimental results. The ^{7}Be production cross section shown in Fig. 6 is derived from experimental data in Table I, excluding the data for the Fe target from the training set. Despite not incorporating the experimental data for the Fe target, our ML model accurately reproduces the experimental results, thanks to the similarity of cross sections with neighboring targets. These figures show that our ML model has good predictive capability for cross sections even in regions where no experimental data exist.

B. ^{3}H production cross sections

Table II presents the EXFOR entry numbers and reference numbers for generating ^{3}H production cross sections, along with the corresponding number of experimental data points for each target. In contrast to the experimental ^{7}Be production
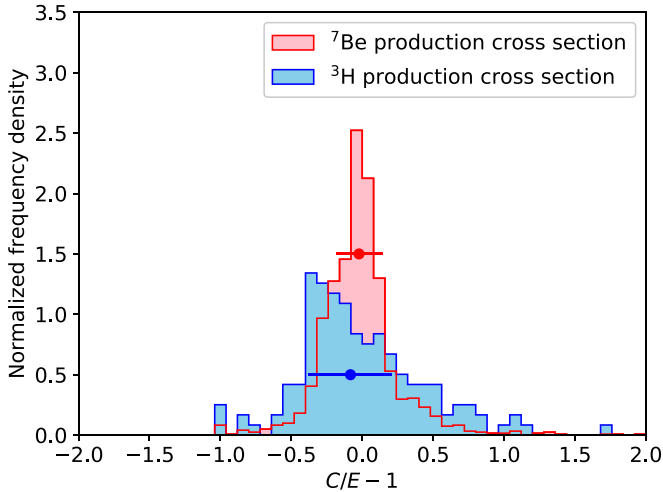
FIG. 8. Normalized frequency density distributions of $C/E - 1$ values for the proton-induced ^{7}Be and ^{3}H production cross sections. Point with error bar indicates median with IQR.

cross-section data (Table I), the experimental ^{3}H production cross-section data consists of only 150 points. However, as illustrated in Fig. 7, our ML model generates plausible cross-section curves. Although the estimation uncertainty would be significant compared to the ^{7}Be production cross-section results due to limited experimental data, the amount of ^{3}H produced increases with both target mass number and incident proton energy for all targets from C to Bi, consistent with the physics model analysis. It is worth noting here that INCL4.6/GEM generally tends to overestimate the ^{3}H production cross sections.

In Fig. 8, the $C/E - 1$ normalized frequency density distributions of the ML model estimates for ^{7}Be and ^{3}H production cross sections are depicted. The ^{7}Be production cross section had a median and interquartile range (IQR) of $(-0.02, 0.25)$, while the ^{3}H production cross section showed (median, IQR) $= (-0.08, 0.53)$. This implies that the $C/E - 1$ values for ^{3}H production cross sections exhibit greater variability compared to ^{7}Be production cross sections. This distribution does not align with the normal distribution generated by GPs, but the widths of both distributions are anticipated to decrease with the inclusion of additional experimental data in the training set, according to Bayes' theorem.

IV. CONCLUSION

In this study, we developed an ML model using GP to estimate nuclide production cross sections in a fully phenomenological manner. The model exhibits the capability to estimate cross sections even in regions with sparse experimental data through transfer learning, assuming the similarity of cross-section shapes between target masses. Using this model, we estimated ^{7}Be and ^{3}H production cross sections from experimental data spanning a wide range of target elements, from C to Bi. The results were compared with both experimental data and physics model analysis, validating the reliability of our ML model.

This paper focused on target elements with natural abundance (e.g., $^{\text{nat}}$Fe), for which experimental data were relatively abundant. However, to estimate nuclide production cross sections for individual target nuclei (e.g., ^{54,56,57,58}Fe) using a phenomenological approach, additional experimental data may be necessary. Additionally, while our primary focus was on nuclide production cross sections, the results suggest the potential applicability of our ML model to various cross sections.

It is important to note that the current ML model is not equipped to handle highly characteristic nuclear reactions, such as nuclear resonances, or cases where the trend changes dramatically for adjacent target nuclei, such as magic isotopes. For such scenarios, physics models serve as a powerful tool for estimating cross sections. The limitation of our ML model lies in its assumption of similarity in cross-section shapes among adjacent target elements in terms of atomic mass. However, this assumption enhances generalization and interpolation performance for various target elements, as demonstrated in this paper. Even for nuclear reactions that lack obvious similarities at first glance, identifying commonalities could facilitate cross-section estimation through a phenomenological approach using transfer learning.

[1] J. W. Norbury, J. Miller, A. M. Adamczyk *et al.*, Nuclear data for space radiation, Radiat. Meas. **47**, 315 (2012).

[2] P. Gondolo, Wanted! Nuclear data for dark matter astrophysics, Nucl. Data Sheets **120**, 175 (2014).

[3] Y. Génolini, D. Maurin, I. V. Moskalenko, and M. Unger, Current status and desired precision of the isotopic production cross sections relevant to astrophysics of cosmic rays: Li, Be, B, C, and N, Phys. Rev. C **98**, 034611 (2018).

[4] J.-C. David and I. Leya, Spallation, cosmic rays, meteorites, and planetology, Prog. Part. Nucl. Phys. **109**, 103711 (2019).

[5] M. Kusakabe and G. J. Mathews, Modern results for the cosmic ray nucleosynthesis of *p*-nuclei, *Proceedings of the 15th International Symposium on Origin of Matter and Evolution of Galaxies* (OMEG15) (Physics Society of Japan, Kyoto, Japan, 2020).

[6] K. Kolos, V. Sobes, R. Vogt *et al.*, Current nuclear data needs for applications, Phys. Rev. Res. **4**, 021001 (2022).

[7] M. S. Smith, Nuclear data resources and initiatives for nuclear astrophysics, Front. Astron. Space Sci. **10**, 1243615 (2023).

[8] H. Iwamoto, K. Nishihara, Y. Iwamoto *et al.*, Impact of PHITS spallation models on the neutronics design of an accelerator-driven system, J. Nucl. Sci. Technol. **53**, 1585 (2016).

[9] A. Stankovskiy, H. Iwamoto, Y. Çelik *et al.*, High-energy nuclear data uncertainties propagated to MYRRHA safety parameters, Ann. Nucl. Energy **120**, 207 (2018).

[10] H. A. Abderrahim, D. De Bruyn, G. Van den Eynde *et al.*, Accelerator driven subcritical systems, in *Encyclopedia of Nuclear Energy*, edited by E. Greenspan (Elsevier, Oxford, 2021), pp. 191–202.

[11] K. Nishihara, H. Iwamoto, and K. Suyama, *Estimation of Fuel Compositions in Fukushima-Daiichi Nuclear Power Plant, JAEA-Data/Code 2012-018* (Japan Atomic Energy Agency, Tokai, Japan, 2012).

[12] W. R. Webber, J. C. Kish, and D. A. Schrier, Formula for calculating partial cross sections for nuclear reactions of nuclei with $E \gtrsim 200$ MeV/nucleon in hydrogen targets, Phys. Rev. C **41**, 566 (1990).

[13] J. Aichelin, "Quantum" molecular dynamics–a dynamical microscopic *n*-body approach to investigate fragment formation and the nuclear equation of state in heavy ion collisions, Phys. Rep. **202**, 233 (1991).

[14] Y. Nara, N. Otuka, A. Ohnishi *et al.*, Relativistic nuclear collisions at $10A$ GeV energies from $p +$ Be to Au + Au with the hadronic cascade model, Phys. Rev. C **61**, 024901 (1999).

[15] A. Ono and H. Horiuchi, Antisymmetrized molecular dynamics for heavy ion collisions, Prog. Part. Nucl. Phys. **53**, 501 (2004).

[16] Y. Watanabe, K. Kosako, S. Kunieda *et al.*, Status of JENDL high energy file, J. Korean Phys. Soc. **59**, 1040 (2011).

[17] C. Schmitt, K.-H. Schmidt, and A. Kelić-Heil, SPACS: A semi-empirical parameterization for isotopic spallation cross sections, Phys. Rev. C **90**, 064605 (2014).

[18] O. Iwamoto, N. Iwamoto, S. Kunieda *et al.*, The CCONE code system and its application to nuclear data evaluation for fission and other reactions, Nucl. Data Sheets **131**, 259 (2016), Special Issue on Nuclear Reaction Data.

[19] S. G. Mashnik, L. M. Kerby, K. K. Gudima *et al.*, Production of energetic light fragments in extensions of the CEM and LAQGSM event generators of the Monte Carlo transport code MCNP6, Phys. Rev. C **95**, 034613 (2017).

[20] S. Okumura, T. Kawano, P. Jaffke *et al.*, ^{235}U(n, f) Independent fission product yield and isomeric ratio calculated with the statistical Hauser–Feshbach theory, J. Nucl. Sci. Technol. **55**, 1009 (2018).

[21] M. Fleming, J.-C. David, J. Rodríguez-Sánchez *et al.*, The high-energy intra-nuclear cascade Liège-based residual (HEIR) nuclear data library, EPJ Web Conf. **239**, 20001 (2020).

[22] T. Kawano, CoH$_3$: The Coupled-Channels and Hauser-Feshbach Code, in *Compound-Nuclear Reactions*, edited by J. Escher, Y. Alhassid, L. A. Bernstein, D. Brown, C. Fröhlich, P. Talou, and W. Younes (Springer International Publishing, Cham, 2021), pp. 27–34.

[23] A. Koning, S. Hilaire, and S. Goriely, TALYS: Modeling of nuclear reactions, Eur. Phys. J. A **59**, 131 (2023).

[24] S. M. Qaim, F. T. Tárkányi, P. Obložinský *et al.*, Charged-particle cross section database for medical radioisotope production, J. Nucl. Sci. Technol. **39**, 1282 (2002).

[25] A. Hermanne, F. Tárkányi, A. Ignatyuk *et al.*, Evaluated and recommended cross-section data for production of radionuclides with emerging interest in nuclear medicine imaging. Part 1: Positron emission tomography (PET), Nucl. Instrum. Methods Phys. Res. B **535**, 149 (2023).

[26] N. Otuka and O. Iwamoto, EXFOR-based simultaneous evaluation of neutron-induced uranium and plutonium fission cross sections for JENDL-5, J. Nucl. Sci. Technol. **59**, 1004 (2022).

[27] C. E. Rasmussen and C. K. I. Williams, *Gaussian Processes for Machine Learning (Adaptive Computation and Machine Learning)* (The MIT Press, Cambridge, MA, 2005).

[28] H. Iwamoto, Generation of nuclear data using Gaussian process regression, J. Nucl. Sci. Technol. **57**, 932 (2020).

[29] H. Iwamoto, O. Iwamoto, and S. Kunieda, G-HyND: A hybrid nuclear data estimator with Gaussian processes, J. Nucl. Sci. Technol. **59**, 334 (2022).

[30] T. Sato, Y. Iwamoto, S. Hashimoto *et al.*, Recent improvements of the particle and heavy ion transport code system–PHITS version 3.33, J. Nucl. Sci. Technol. **61**, 127 (2023).

[31] S. Furihata, Statistical analysis of light fragment production from medium energy proton-induced reactions, Nucl. Instrum. Methods Phys. Res. B **171**, 251 (2000).

[32] A. Boudard, J. Cugnon, J.-C. David *et al.*, New potentialities of Liège intranuclear cascade model for reactions induced by nucleons and light charged particles, Phys. Rev. C **87**, 014606 (2013).

[33] L. Sihver, D. Mancusi, K. Niita *et al.*, Benchmarking of calculated projectile fragmentation cross-sections using the 3-D, MC codes PHITS, FLUKA, HETC-HEDS, MCNPX_HI, and NUCFRG2, Acta Astronaut. **63**, 865 (2008).

[34] Y. Iwamoto, T. Sato, S. Hashimoto *et al.*, Benchmark study of the recent version of the PHITS code, J. Nucl. Sci. Technol. **54**, 617 (2017).

[35] H. Iwamoto, S. Meigo, D. Satoh, *et al.*, Neutron-production double-differential cross sections of ^{nat}Pb and ^{209}Bi in proton-induced reactions near 100 MeV, Nucl. Instrum. Methods Phys. Res. B **544**, 165107 (2023).

[36] H. Iwamoto, K. Nakano, S. Meigo *et al.*, Measurement of 107-MeV proton-induced double-differential thick target neutron yields for Fe, Pb, and Bi using a fixed-field alternating gradient accelerator at Kyoto University, J. Nucl. Sci. Technol. **60**, 435 (2023).

[37] N. Otuka, E. Dupont, V. Semkova *et al.*, Towards a more complete and accurate experimental nuclear reaction data library (EXFOR): International collaboration between Nuclear Reaction Data Centres (NRDC), Nucl. Data Sheets **120**, 272 (2014).

[38] K. Nakano, H. Matsuda, S. Meigo *et al.*, Measurement of Nuclide Production Cross-sections in High-energy Proton-induced Spallation Reactions at J-PARC, JAEA-Research 2021-014 (Japan Atomic Energy Agency, 2022).

[39] K. Sugihara, S. Meigo, H. Iwamoto *et al.*, Measurement of nuclide production cross sections for proton-induced reactions on ^{nat}Ti and ^{93}Nb at 0.8 and 3.0 GeV, Nucl. Instrum. Methods Phys. Res. B **545**, 165153 (2023).

[40] D. Brown, M. Chadwick, R. Capote *et al.*, ENDF/B-VIII.0: The 8th major release of the nuclear reaction data library with CIELO-project cross sections, new standards and thermal scattering data, Nucl. Data Sheets **148**, 1 (2018), Special Issue on Nuclear Reaction Data.

[41] O. Iwamoto, N. Iwamoto, S. Kunieda *et al.*, Japanese evaluated nuclear data library version 5: JENDL-5, J. Nucl. Sci. Technol. **60**, 1 (2023).

[42] C. Zhu, R. H. Byrd, P. Lu *et al.*, Algorithm 778: L-BFGS-B: Fortran subroutines for large-scale bound-constrained optimization, ACM Trans. Math. Softw. **23**, 550 (1997).

[43] M. Honda and D. Lal, Some cross sections for the production of radio-nuclides in the bombardment of C, N, O, and Fe by medium energy protons, Phys. Rev. **118**, 1618 (1960).

[44] E. Baker, G. Friedlander, and J. Hudis, Formation of Be^7 in interaction of various nuclei with high-energy protons, Phys. Rev. **112**, 1319 (1958).

[45] J. B. Cumming, G. Friedlander, J. Hudis, and A. M. Poskanzer, Spallation of aluminum by 28-GeV protons, Phys. Rev. **127**, 950 (1962).

[46] I. Leya, Modelling of the interactions between galactic cosmic rays with stone and iron meteorites - Thin-target irradiations and thick-target experiments, Ph.D. thesis, 1997.

[47] G. V. S. Rayudu, Formation cross sections of various radionuclides from Ni, Fe, Si, Mg, O and C for protons of energies between 130 and 400 MeV, Can. J. Chem. **42**, 1149 (1964).

[48] R. Michel, M. Gloris, H. J. Lange, *et al.*, Nuclide production by proton-induced reactions on elements ($6 \leqslant Z \leqslant 29$) in the energy range from 800 to 2600 MeV, Nucl. Instrum. Methods Phys. Res. B **103**, 183 (1995).

[49] T. Schiekel, F. Sudbrock, U. Herpers *et al.*, Nuclide production by proton-induced reactions on elements ($6 \leqslant Z \leqslant 29$) in the energy range from 200 MeV to 400 MeV, Nucl. Instrum. Methods Phys. Res. B **114**, 91 (1996).

[50] M. Fassbender, B. Scholten, and S. M. Qaim, Radiochemical studies of (p,^{7}Be) reactions on biologically relevant elements in the proton energy range of 50 to 350 MeV, Radiochim. Acta **81**, 1 (1998).

[51] C. M. Backer, C. Baumer, M. Gerhardt *et al.*, Measurement of nuclear activation cross sections of protons on natural carbon for proton beam energies between 100 and 220 MeV, Nucl. Instrum. Methods Phys. Res. B **454**, 50 (2019).

[52] V. N. Aleksandrov, M. P. Semenova, and V. G. Semenov, The production of Be-7 at middle energy protons interaction with light nuclei., Vopr. Atomn. Nauki i Tekhn., Ser. Yad. Fiz. Issledo., 17 (1990).

[53] R. Bodemann, H. J. Lange, I. Leya *et al.*, Production of residual nuclei by proton-induced reactions on C, N, O, Mg, Al and Si, Nucl. Instrum. Methods Phys. Res. B **82**, 9 (1993).

[54] M. Barbier and S. Regnier, Production of ^{7}Be from light targets by 30 MeV to 24 GeV protons, J. Inorg. Nucl. Chem. **33**, 2720 (1971).

[55] Y. Parrat, W. Hajdas, U. Baltensperger *et al.*, Cross section measurements of proton induced reactions using a gas target, Nucl. Instrum. Methods Phys. Res. B **113**, 470 (1996).

[56] J. L. Reyss, Y. Yokoyama, and F. Guichard, Production cross sections of ^{26}Al, ^{22}Na, ^{7}Be from Argon and of ^{10}Be, ^{7}Be from Nitrogen: Implications for production rates of ^{26}Al and ^{10}Be in the atmosphere, Earth Planet. Sci. Lett. **53**, 203 (1981).

[57] G. M. Raisbeck and F. Yiou, The Be-10 problem revisited, *15th International Cosmic Ray Conference* (Plovdiv, Bulgaria, 1977), p. 203.

[58] L. Valentin, G. Albouy, J. P. Cohen, and M. Gusakow, Reactions induites par des protons de 155 MeV sur des noyaux legers, Phys. Lett. **7**, 163 (1963).

[59] P. A. Benioff, Nuclear reactions of low-Z elements with 5.7-BeV protons, Phys. Rev. **119**, 316 (1960).

[60] R. Michel, R. Bodemann, H. Busemann *et al.*, Cross sections for the production of residual nuclides by low- and medium-energy protons from the target elements C, N, O, Mg, Al, Si, Ca, Ti, V, Mn, Fe, Co, Ni, Cu, Sr, Y, Zr, Nb, Ba and Au, Nucl. Instrum. Methods Phys. Res. B **129**, 153 (1997).

[61] R. Bimbot and H. Gauvin, Reactions de spallation de noyaux legers induites par des protons de 50, 100 et 153 MeV, Comptes Rendus, Série B, Physique **273**, 1054 (1971).

[62] E. S. Izosimova, A. A. Nosov, V. V. Smirnov *et al.*, Be-7 Production cross sections in light nuclei disintegration by protons of 0.66 and 1.0 GeV, Progress Report No. 87 (1978) Khlopin Radiev. Institute, Leningrad Reports.

[63] J. M. Sisterson, K. Kim, A. Beverding *et al.*, Measuring excitation functions needed to interpret cosmogenic nuclide production in lunar rocks, *Application of Accelerators in Research and Industry*, Denton, USA, 1996.

[64] R. H. Lindsay and E. F. Neuzil, (p, Be^7) reaction in Al and Mg from 27 to 31.5 MeV, Phys. Rev. **127**, 1269 (1962).

[65] G. V. S. Rayudu, Formation cross sections of various radionuclides from Ni, Fe, Si, Mg, O and C for protons of energies between 0.5 and 2.9 GeV, J. Inorg. Nucl. Chem. **30**, 2311 (1968).

[66] R. Michel, B. Dittrich, U. Herpers *et al.*, Proton-induced spallation at 600 MeV, Analyst (London) **114**, 287 (1989).

[67] G. M. Raisbeck and F. Yiou, Production cross sections for ^{7}Be and ^{22}Na in targets of Si, Mg, Fe, and Ni irradiated by 1, 2, 3, and 23 GeV protons, Phys. Rev. C **12**, 915 (1975).

[68] H. R. Heydegger, A. L. Turkevich, A. Van Ginneken *et al.*, Production of ^{7}Be, ^{22}Na, and ^{28}Mg from Mg, Al, and SiO$_2$ by protons between 82 and 800 MeV, Phys. Rev. C **14**, 1506 (1976).

[69] G. M. Raisbeck and F. Yiou, Cross sections for the spallation production of ^{10}Be in targets of N, Mg, and Si and their astrophysical applications, Phys. Rev. C **9**, 1385 (1974).

[70] V. N. Aleksandrov, M. P. Semenova, and V. G. Semenov, Cross sections of radionuclide production in (p,X)-reactions, Atomnaya Energiya **64**, 445 (1988).

[71] Y. E. Titarenko, S. P. Borovlev, M. A. Butko *et al.*, Cross sections for monitor reactions ^{27}Al(p, x) ^{24}Na, ^{27}Al(p, x) ^{22}Na, and ^{27}Al(p, x) ^{7}Be at proton energies in the range 0.04–2.6 GeV, Phys. At. Nucl. **74**, 507 (2011).

[72] A. K. Lavrukhina, L. P. Moskaleva, V. V. Malyshev *et al.*, Production of light nuclei by bombarding heavy elements with 660 MeV protons, J. Exp. Theor. Phys. **16**, 1 (1963).

[73] J. E. Cline and E. B. Nieschmidt, Measurements of spallation cross sections for 590 MeV protons on thin targets of copper, nickel, iron and aluminum, Nucl. Phys. A **169**, 437 (1971).

[74] E. F. Neuzil and R. H. Lindsay, Emission of Be^7 and competition processes at 30 to 42 MeV, Phys. Rev. **131**, 1697 (1963).

[75] T. N. Taddeucci, J. Ullmann, L. J. Rybarcyk *et al.*, Total cross sections for production of ^{7}Be, ^{22}Na, and ^{24}Na in p + ^{7}Li and p + ^{27}Al reactions at 495 and 795 MeV, Phys. Rev. C **55**, 1551 (1997).

[76] S. B. Kaufman, M. W. Weisfield, E. P. Steinberg *et al.*, Spallation of aluminum by 300 GeV protons, Phys. Rev. C **19**, 962 (1979).

[77] A. Grutter, Cross sections for reactions with 593 and 540 MeV protons in aluminium, arsenic, bromine, rubidium and yttrium, Appl. Radiat. Isot. **33**, 725 (1982).

[78] B. Scholten, S. M. Qaim, and G. Stocklin, Radiochemical studies of proton induced ^{7}Be-emission reactions in the energy range of 40 to 100 MeV, Radiochim. Acta **65**, 81 (1994).

[79] A. Grutter, Excitation functions for radioactive isotopes produced by proton bombardment of Cu and Al in the energy range of 16 to 70 MeV, Nucl. Phys. A **383**, 98 (1982).

[80] F. Szelecsenyi, G. F. Steyn, F. M. Nortier, and Z. Kovacs, New cross sections for the ^{27}Al(p, x) ^{7}Be nuclear process: Monitoring proton beam energy via the ^{22}Na $/$ ^{7}Be cross-section ratio between 45 and 200 MeV, EPJ Web Conf. **146**, 08011 (2017).

[81] M. S. Lafleur, N. T. Porile, and L. Yaffe, Formation of ^{7}Be in nuclear reactions induced by 85-MeV protons, Can. J. Chem. **44**, 2749 (1966).

[82] K. Miyano, The ^{7}Be, ^{22}Na and ^{24}Na production cross sections with 52- to 22-MeV proton on ^{27}Al, J. Phys. Soc. Jpn. **34**, 853 (1973).

[83] H. Yashima, Y. Uwamino, H. Sugita *et al.*, Projectile dependence of radioactive spallation products induced in copper by high-energy heavy ions, Phys. Rev. C **66**, 044607 (2002).

[84] H. Matsuda, S. Meigo, and H. Iwamoto, Proton-induced activation cross section measurement for aluminum with proton energy range from 0.4 to 3 GeV at J-PARC, J. Nucl. Sci. Technol. **55**, 955 (2018).

[85] H. Matsuda, S. Meigo, and H. Iwamoto, Measurement of activation cross sections of aluminum for protons with energies between 0.4 GeV and 3.0 GeV at J-PARC, Prog. Nucl. Sci. Technol. **6**, 171 (2019).

[86] L. P. Moskaleva, G. A. Fedoseev, and A. N. Khalemskii, Yields of the isotopes Be^{7}, C^{11}, F^{18}, Na^{22}, ^{24} in bombardment of aluminum by 30-, 50-, and 70-BeV protons, Sov. J. Nucl. Phys. **12**, 472 (1971).

[87] Y. E. Titarenko, O. V. Shvedov, V. F. Batyaev *et al.*, Experimental and theoretical study of the yields of radioactive product nuclei in Tc-99 thin targets irradiated with 100-2600 MeV protons, Technical Report No. 434 (2002), USSR report to the I.N.D.C.

[88] Y. E. Titarenko, V. F. Batyaev, R. D. Mulambetov *et al.*, Excitation functions of product nuclei from 40 to 2600 MeV proton-irradiated $^{206,207,208,\mathrm{nat}}$Pb and ^{209}Bi, Nucl. Instrum. Methods Phys. Res. A **562**, 801 (2006).

[89] M. Ligonniere, B. Vassent, and R. Bernas, Production cross section of beryllium-7 from Al, V, Ta and Au induced by 155 and 550 MeV protons, Comptes Rendus **259**, 1406 (1964).

[90] J. M. Sisterson, K. Kim, A. Beverding *et al.*, Measurement of proton production cross sections of ^{10}Be and ^{26}Al from elements found in lunar rocks, Nucl. Instrum. Methods Phys. Res. B **123**, 324 (1997).

[91] S. Regnier, P. Paillard, and G. Simonoff, Production de beryllium-7 dans le fer et le silicium par des protons de 0.6 et 24 GeV, Comptes Rendus, Serie B, Physique **280**, 513 (1975).

[92] Y. T. Mironov, A. A. Aleksandrov, and S. D. Golos, Yields of nuclei at bombardment Ar by protons with energy 1 GeV, Prikladnaya Yadernaya Spektroskopiya **7**, 211 (1977).

[93] R. L. Brodzinski and N. A. Wogman, High-energy proton spallation of argon, Phys. Rev. C **1**, 1955 (1970).

[94] Y. V. Aleksandrov, A. I. Bogdanov, S. K. Vasilev *et al.*, Cross section for the production of radioactive nuclides under bombardment of intermediate-mass nuclei with 1-GeV protons, Izv. Rossiiskoi Akademii Nauk, Ser. Fiz. **54**, 2249 (1990).

[95] Y. V. Aleksandrov, S. K. Vasiliev, R. B. Ivanov *et al.*, Cross sections for spallation production of radioactive nuclides by 660 MeV protons, Bull. Russian Academy of Sciences - Physics **59**, 895 (1995).

[96] R. L. Brodzinsk, L. A. Rancitelli, J. A. Cooper, and N. A. Wogman, High-energy proton spallation of titanium, Phys. Rev. C **4**, 1250 (1971).

[97] S. Neumann, Activation experiments with medium-energy neutrons and the production of cosmogenic nuclides in extraterrestrial matter, Ph.D. thesis, 1999.

[98] L. Husain and S. Katcoff, Interaction of 3- and 29-GeV protons with vanadium, Phys. Rev. C **7**, 2452 (1973).

[99] Y. E. Titarenko, V. F. Batyaev, A. Y. Titarenko *et al.*, Measurement and simulation of the cross sections for nuclide production in ^{56}Fe and $^{\mathrm{nat}}$Cr targets irradiated with 0.04- to 2.6-GeV protons, Phys. At. Nucl. **74**, 523 (2011).

[100] H. Takeshita, S. Meigo, H. Matsuda *et al.*, Measurement of nuclide production cross sections for proton-induced reactions on Mn and Co at 1.3, 2.2, and 3.0 GeV, Nucl. Instrum. Methods Phys. Res. B **511**, 30 (2022).

[101] C. Perrin, Cross sections for production of stable and long-lived nuclides by high energy spallation of iron: Cosmic ray implications, Phys. Rev. C **14**, 1108 (1976).

[102] A. K. Lavrukhina, L. D. Revina, V. V. Malyshev *et al.*, Spallation of Fe nuclei induced by 150 MeV protons, J. Exp. Theor. Phys. **17**, 960 (1963).

[103] A. K. Lavrukhina, L. D. Revina, V. V. Malyshev *et al.*, Further investigation of the products of the spallation of iron by 660 MeV protons, Sov. Radiochem. **5**, 682 (1963).

[104] M. Gloris, Proton-induced production of residual nuclei in heavy elements at medium energies, Ph.D. thesis, 1998.

[105] C. J. Orth, H. A. O'Brien Jr., M. E. Schillaci *et al.*, Interlaboratory comparison of spallation-reaction cross sections for iron and copper with 590-MeV protons, J. Inorg. Nucl. Chem. **38**, 13 (1976).

[106] S. Katcoff, S. B. Kaufman, E. P. Steinberg *et al.*, Nuclear reactions of V with 300-GeV protons and Co with 11.5-, 200-, and 300-GeV protons, Phys. Rev. Lett. **30**, 1221 (1973).

[107] Y. E. Titarenko, E. I. Karpikhin, A. F. Smolyakov *et al.*, Experimental and Calculative Research of Radioactive Nuclei Formation-Products of Target and Constructional Materials of Electronuclear Facilities Irradiated by Protons with Energies 1.5 GeV and 130 MeV, Workshop on Exact Measurements in Nuclear Spectroscopy, Sarov, Russia 1996, p. 184.

[108] Y. E. Titarenko, V. F. Batyaev, A. Y. Titarenko *et al.*, Measurement and simulation of the cross sections for nuclide production in ^{93}Nb and $^{\mathrm{nat}}$Ni targets irradiated with 0.04- to 2.6-GeV protons, Phys. At. Nucl. **74**, 537 (2011).

[109] H. Takeshita, S. Meigo, H. Matsuda *et al.*, Measurement of nuclide production cross sections for proton-induced reactions on $^{\mathrm{nat}}$Ni and $^{\mathrm{nat}}$Zr at 0.4, 1.3, 2.2, and 3.0 GeV, Nucl. Instrum. Methods Phys. Res. B **527**, 17 (2022).

[110] G. M. Raisbeck, P. Boerstling, R. Klapisch *et al.*, Li, Be, and B production in the 3-GeV proton bombardment of Ni, Phys. Rev. C **12**, 527 (1975).

[111] J. B. Cumming, P. E. Haustein, R. W. Stoenner *et al.*, Spallation of Cu by 3.9-GeV ^{14}N ions and 3.9-GeV protons, Phys. Rev. C **10**, 739 (1974).

[112] M. Fassbender, Y. N. Shubin, V. P. Lunev *et al.*, Experimental studies and nuclear model calculations on the formation of radioactive products in interactions of medium energy protons with copper, zinc and brass: Estimation of collimator activation in proton therapy facilities, Appl. Radiat. Isot. **48**, 1221 (1997).

[113] T. Asano, Y. Asano, Y. Iguchi *et al.*, Target dependence of charge distributions in spallation reactions of medium-mass nuclei with 12 GeV protons, Phys. Rev. C **28**, 1718 (1983).

[114] Y. Asano, S. Mori, M. Sakano *et al.*, Nuclear reactions of Ti, Fe, Co, Ni, Cu, and Zn by 500-MeV protons, J. Phys. Soc. Jpn. **60**, 107 (1991).

[115] S. Regnier, B. Lavielle, M. Simonoff, and G. N. Simonoff, Nuclear reactions in Rb, Sr, Y, and Zr targets, Phys. Rev. C **26**, 931 (1982).

[116] Y. V. Aleksandrov, A. A. Astapov, S. K. Vasilev *et al.*, Production Cross Sections for Nuclides in Zirconium Target Bombarded by Protons with Energy 660 MeV, 41. Nuclear Spectroscopy and Nuclear Structure, Minsk 1991, p. 488.

[117] R. Wolfle and S. M. Qaim, ^{7}Be emission cross sections in high energy proton induced reactions on ^{51}V, ^{93}Nb and ^{197}Au, Radiochim. Acta **50**, 185 (1990).

[118] Y. E. Titarenko, V. F. Batyaev, E. I. Karpikhin *et al.*, Experimental yields for Nb-93 irradiated with 2.6 GeV protons, Technical Report No. 0434 (2002), USSR report to the I.N.D.C.

[119] Y. V. Aleksandrov, A. A. Astapov, S. K. Vasilev *et al.*, Cross section of (p,X) reactions on molybdenum target at $E_p = 660$ MeV, *International Conference on Nuclear Spectroscopy and Nuclear Structure* (Alma-Ata, Kazakhstan, 1992), p. 446.

[120] C. F. Wang and N. T. Porile, Nuclear reactions of silver with 0.8-TeV protons, Phys. Rev. C **33**, 2183 (1986).

[121] G. English, Y. W. Yu, and N. T. Porile, Nuclear reactions of silver with 300-GeV protons, Phys. Rev. C **10**, 2281 (1974).

[122] G. English, N. T. Porile, and E. P. Steinberg, Nuclear reactions of silver with 11.5-GeV protons, Phys. Rev. C **10**, 2268 (1974).

[123] E. N. Volnin, A. A. Vorobev, and D. M. Seliverstov, Production of light fragments in the interaction of 1-GeV protons with silver nuclei, Zhurnal Eksper. i Teoret. Fiz., Pisma v Redakt. **19**, 691 (1974).

[124] D. R. Nethaway and L. Winsberg, Interaction of high-energy protons with indium, Phys. Rev. **119**, 1375 (1960).

[125] S. A. Karamian, C. A. Ur, J. Adam *et al.*, Spallation and fission products in the (p + ^{179}Hf) and (p + ^{nat}Hf) reactions, Nucl. Instrum. Methods Phys. Res. A **600**, 488 (2009).

[126] Y. E. Titarenko, V. F. Batyaev, A. Y. Titarenko *et al.*, Measurement and simulation of the cross sections for nuclide production in ^{nat}W and ^{181}Ta targets irradiated with 0.04- to 2.6-GeV protons, Phys. At. Nucl. **74**, 551 (2011).

[127] Y. E. Titarenko, O. V. Shvedov, V. F. Batyaev *et al.*, Study of residual product nuclide yields in 1-GeV proton irradiated Pb-208 and 2.6-GeV proton irradiated W-natural thin target, Technical Report No. 00-3597 (2000), Los Alamos Scientific Laboratory Reports.

[128] Y. E. Titarenko, V. F. Batyaev, E. I. Karpikhin *et al.*, Experimental yields for W-nat irradiated with 2.6 GeV protons, Technical Report No. 434 (2002), USSR report to the I.N.D.C.

[129] S. A. Karamian, J. Adam, P. Chaloun *et al.*, Yield of radionuclides and isomers produced in the fragmentation on ^{nat}W and ^{186}W (97%) targets with protons at 630, 420 and 270 MeV, Nucl. Instrum. Methods Phys. Res. A **527**, 609 (2004).

[130] R. Michel, M. Gloris, J. Protoschill *et al.*, Cross section for the production of radionuclides by Proton-induced reactions on W, Ta, Pb, and Bi from thresholds up to 2.6 GeV, J. Nucl. Sci. Technol. Suppl. **39**, 242 (2002).

[131] S. A. M. Issa, M. A. M. Uosif, R. Michel *et al.*, Proton-induced production of residual radionuclides in ^{nat}Re up to 2590 MeV, Nucl. Instrum. Methods Phys. Res. B **298**, 19 (2013).

[132] Y. E. Titarenko, V. F. Batyaev, M. A. Butko *et al.*, Verification of high-energy transport codes on the basis of activation data, Phys. Rev. C **84**, 064612 (2011).

[133] M. Gloris, R. Michel, F. Sudbrock *et al.*, Proton-induced production of residual radionuclides in lead at intermediate energies, Nucl. Instrum. Methods Phys. Res. A **463**, 593 (2001).

[134] V. N. Mekhedov, Formation of tritium in C, Al and Fe under the influence of protons with $E_p = 130$-660 MeV, Yad. Fiz. **5**, 34 (1967) [Sov. J. Nucl. Phys. **5**, 24 (1967)].

[135] L. A. Currie, Tritium production by 6-Bev protons, Phys. Rev. **114**, 878 (1959).

[136] P. C. Brun, M. Lefort, and X. Tarrago, Contribution a l'etude du double pick-up indirect mesure de la production de tritium par des protons de 82 et 105 MeV dans diverses cibles, J. Phys. Radium **23**, 167 (1962).

[137] L. A. Currie, W. F. Libby, and R. L. Wolfgang, Tritium production by high-energy protons, Phys. Rev. **101**, 1557 (1956).

[138] V. V. Kuznetsov and V. N. Mekhedov, Tritium production in metals by 120 to 600-MeV protons, J. Exp. Theor. Phys. **8**, 406 (1959).

[139] K. Goebel and J. Zähringer, Erzeugung von tritium und edelgasisotopen bei besstrahlung von Fe und Cu mit protonen von 25 GeV energie, Z. Naturforsch. A **16**, 231 (1961).

[140] J. Gonzalez-Vidal and W. H. Wade, Survey of tritium-producing nuclear reactions, Phys. Rev. **120**, 1354 (1960).

[141] Y. E. Titarenko, M. V. Chauzova, K. V. Pavlov *et al.*, Cross section of tritium production in structural materials of accelerator-driven facilities, Phys. At. Nucl. **84**, 1697 (2021).

[142] B. N. Mekhedov and V. N. Mekhedov, Production of tritium in Al, Sn, Pb, and Bi under the influence of high-energy protons, Sov. J. Nucl. Phys. **11**, 397 (1970).

[143] M. Noguchi, T. Miura, K. Kondo *et al.*, Production cross sections of tritium in high energy nuclear reactions with 12 GeV protons, Appl. Radiat. Isot. **42**, 577 (1991).

[144] M. Lefort, G. N. Simonoff, and X. Tarrago, A spallation nuclear reaction on thorium at 150 and 82 proton energies, Nucl. Phys. **25**, 216 (1961).

[145] S. T. Kruger and D. Heymann, High-energy proton production of ^{3}H, ^{3}He, and ^{4}He in light targets, Phys. Rev. C **7**, 2179 (1973).

[146] O. A. Schaeffer and J. Zähringer, High-sensitivity mass spectrometric measurement of stable helium and argon isotopes produced by high-energy protons in Iron, Phys. Rev. **113**, 674 (1959).

[147] K. Goebel, Tritium production in iron by protons at energies between 50 and 177 MeV, Technical Report No. 58-2 (1958), CERN European Organisation for Nuclear Research Reports.

[148] A. Budzanowski, M. Fidelus, D. Filges *et al.*, Competition of coalescence and "fireball" processes in nonequilibrium emission of light charged particles from p + Au collisions, Phys. Rev. C **78**, 024603 (2008).